Modeling of non-equilibrium phenomena in expanding flows by means of a collisional-radiative model

Alessandro Munafo, Andrea Lani, Arnaud Bultel, Marco Panesi

Modeling of non-equilibrium phenomena in expanding flows by means of a collisional-radiative model

A. Munafò,[1,a)] A. Lani,[1,b)] A. Bultel,[2,c)] and M. Panesi[3,d)]
[1]*Aeronautics and Aerospace Department, von Karman Institute for Fluid Dynamics, Chaussée de Waterloo 72, 1640 Rhode-Saint-Genèse, Belgium*
[2]*CORIA, UMR CNRS 6614, Université de Rouen, Site universitaire du Madrillet, Avenue de l'Université 76801 Saint-Etienne du Rouvray Cedex, France*
[3]*Aerospace Department, University of Illinois at Urbana-Champaign, 306 Talbot Lab, 104 S. Wright St., Urbana, Illinois 61801, USA*

(Received 12 January 2013; accepted 29 April 2013; published online 10 July 2013)

The effects of non-equilibrium in a quasi-one-dimensional nozzle flow are investigated by means of a collisional-radiative model. The gas undergoing the expansion is an air plasma and consists of atoms, molecules, and free electrons. In the present analysis, the electronic excited states of atomic and molecular species are treated as separate pseudo-species. Rotational and vibrational energy modes are assumed to be populated according to Boltzmann distributions. The coupling between radiation and gas dynamics is accounted for, in simplified manner, by using escape factors. The flow governing equations for the steady quasi-one-dimensional flow are written in conservative form and discretized in space by means of a finite volume method. Steady-state solutions are obtained by using a fully implicit time integration scheme. The analysis of the evolution of the electronic distribution functions reveals a substantial over-population of the high-lying excited levels of atoms and molecules in correspondence of the nozzle exit. The influence of optical thickness is also studied. The results clearly demonstrate that the radiative transitions, within the optically thin approximation, drastically reduce the over-population of high-lying electronic levels.
 [http://dx.doi.org/10.1063/1.4810787]

I. INTRODUCTION

Converging-diverging nozzles constitute a fundamental component of high enthalpy facilities.[1] Their role is to allow for the expansion of high temperature gases in order to re-create flow environments as close as possible to the conditions encountered by space vehicles during a planetary entry. When the gas expands, its thermal energy is converted into macroscopic kinetic energy leading to an increase in velocity and a decrease in density, pressure, and temperature. Simultaneous recombination of ions, electrons and neutral atoms also occurs. The thermo-chemical state of the gas at the nozzle outlet can have an important impact on the experimental investigation and in some cases can lead to the erroneous duplication of the in-flight environment. For example, the shock stand-off distance and pressure distribution over the model to be tested are strongly influenced by the composition and extent of excitation of the internal energy modes in the test gas. Thus, the correct estimation of the flow conditions is of paramount importance for a correct interpretation of the experimental results and their extrapolation to in-flight conditions. This task is complicated by the non-equilibrium effects occurring when the time-scales of collisional processes become comparable to the macroscopic time-scales of the flow. In nozzles, these conditions are met in the throat region, where the gas expansion becomes significant.[2] As a consequence, the velocity, temperature, and recombination rates are reduced, if compared to an equilibrium expansion. Moreover, populations of species internal degrees of freedom can experience departures from a Boltzmann distribution. A precise estimation of nozzle outlet conditions can be achieved by means of an accurate modeling of gas phase collisional and radiative processes. Concentration of the gas species and distribution of their internal energy level populations can be estimated by means of either multi-temperature models or collisional-radiative (CR) models.

Multi-temperature models[3] were proposed as a simple approach to overcome all difficulties related to the modeling of non-equilibrium flows. They are constructed by prescribing distinct temperatures for the various internal energy modes, assumed to be populated according to Boltzmann distributions. Multi-temperature models are valid only in case of small departures from equilibrium.[4] However, they are widely used outside of their range of validity because of the lack of more accurate physical models, the simplicity of their implementation, and their manageable computational cost.

Collisional-Radiative models[5–11] treat each energy level as a separate pseudo-species. This approach provides more flexibility and accuracy, since it allows for the distribution of the internal energy levels to depart from the equilibrium. However, they require the knowledge of a large number of transition probabilities and elementary reaction rate coefficients to model the kinetic and radiative interactions among each internal energy level. Also, the number of equations to be solved rapidly increases with the number of internal energy levels explicitly included in the kinetic model.

[a)]Electronic mail: munafo@vki.ac.be
[b)]Electronic mail: lani@vki.ac.be
[c)]Electronic mail: arnaud.bultel@coria.fr
[d)]Corresponding author. Electronic mail: mpanesi@illinois.edu

Applications of collisional-radiative models to 2D problems have become feasible only recently.[12–15]

This paper focuses on the application of an electronically specific CR model for ionized air[5,6,10] to non-equilibrium expanding nozzle flows. The CR model in use has been already validated, for the case of compressing flows behind normal shock waves, by means of comparison with spectroscopic measurements performed in the EAST (Electric-Arc-Shock-Tube) facility of NASA Ames Research Center.[16] The main objective of this investigation consists in the analysis of the dynamics of the electronic levels of atoms and molecules. Computations are performed for the steady flow within a realistic nozzle geometry, such as the one of the minitorch facility at the von Karman Institute (VKI). The flow inside the nozzle is considered inviscid and quasi-one-dimensional. These simplifying assumptions, while allowing for the main characteristics of the expansion to be retained, make the computations significantly cheaper, thus, allowing for the use of more accurate physical models.

The manuscript is arranged as follows: Sec. II describes the physical model. The quasi-one-dimensional nozzle flow governing equations are given in Sec. III, while the numerical method is outlined in Sec. IV. Computational results are presented and discussed in Sec. V. Conclusions are given in Sec. VI.

II. PHYSICAL MODELING

A. General considerations and assumptions

The accurate description of an air plasma flow by means of a fully consistent CR model would require the explicit treatment of each internal energy level of the gas species (each individual electronic and rovibronic level for atoms and molecules, respectively) as a separate pseudo-species. Possible deviations of the free electron velocity distribution function from a local Maxwellian should also be taken into account.[9] In addition, the mutual influence between the radiation field and the gas-dynamics should be consistently described through a coupled solution of the radiative transfer and the flow governing equations.[17] The latter represents a formidable computational task. It is for this reason that simplifying assumptions, concerning the kinetic and thermodynamic description of the plasma, are introduced:

1. The translational and rotational (for molecules only) degrees of freedom of heavy-particles are supposed to be in equilibrium at a common temperature T.
2. The velocity distribution function of the free electrons is supposed to be locally Maxwellian at its own temperature T_e. In general, in non-equilibrium flows, T_e is different from the translational temperature of heavy-particles T because of the inefficient energy exchange process caused by the great mass disparity between free electrons and heavy-particles.
3. The presence of thermal non-equilibrium between translation of heavy-particles and electrons and vibration of molecules is described by means of a multi-temperature approach. This means that vibrational levels of a generic molecule m are supposed to be populated according to a Boltzmann distribution at the temperature T_m^{v} (in general, different from T and T_e). The present assumption holds, in general, for the vibrational levels lying close to the ground state, while it gives a less accurate description for high-lying vibrational levels.[9,18]
4. The electronic levels of heavy-particles are treated as separate pseudo-species in order to account for the presence of possible non-Boltzmann distributions. In absence of kinetic data for transitions involving the electronic levels of a given chemical component, its electronic levels are supposed to be populated according to a Boltzmann distribution at the temperature T_e (i.e., in thermal equilibrium with free electrons).
5. The coupling between the radiation field and the gas-dynamics is realized by means of escape factors associated to radiative transitions.

To facilitate the discussion, the following definitions are introduced:

1. $\mathcal{S}$ indicates the set of the species included in the mixture.
2. $\mathcal{S}_{\mathrm{H}}$ indicates the heavy-particle species subset.
3. The subset of electronic energy levels assumed in equilibrium with free electrons is indicated with the $\mathcal{S}_{\mathrm{H}}^{\mathrm{B}}$ symbol (where B stands for Boltzmann).
4. The subset of electronic energy levels treated as separate pseudo-species is indicated with the symbol $\mathcal{S}_{\mathrm{H}}^{\mathrm{NB}}$ (where NB stands for non Boltzmann).
5. The subset of molecular species is indicated with $\mathcal{S}_{\mathrm{M}}$.
6. The set of collisional and radiative processes accounted for $\mathcal{S}_{\mathrm{CR}}$.

Clearly, the subsets $\mathcal{S}_{\mathrm{H}}$, $\mathcal{S}_{\mathrm{H}}^{\mathrm{B}}$, and $\mathcal{S}_{\mathrm{H}}^{\mathrm{NB}}$ satisfy the relation $\mathcal{S}_{\mathrm{H}} = \mathcal{S}_{\mathrm{H}}^{\mathrm{NB}} \cup \mathcal{S}_{\mathrm{H}}^{\mathrm{B}}$.

B. Air mixture

The electronically specific CR model[5] for ionized air used in this work accounts for the following neutral and charged species:

- Neutral species: $\mathrm{N}(1-46)$, $\mathrm{O}(1-40)$, $\mathrm{N_2}(1-4)$, $\mathrm{NO}(1-5)$, and $\mathrm{O_2}(1-5)$.
- Charged species: $\mathrm{e^-}$, $\mathrm{N^+}$, $\mathrm{O^+}$, $\mathrm{N_2^+}(1-4)$, $\mathrm{NO^+}(1-5)$, and $\mathrm{O_2^+}(1-4)$,

where the parentheses are used to identify the electronic levels of a particular chemical component (such as $\mathrm{N_2}$) treated as separate pseudo-species. Thus, according to the definitions introduced in Sec. II A,

$$\mathcal{S} = \{\mathrm{e^-}\} \cup \mathcal{S}_{\mathrm{H}}, \tag{1}$$

$$\mathcal{S}_{\mathrm{H}} = \mathcal{S}_{\mathrm{H}}^{\mathrm{B}} \cup \mathcal{S}_{\mathrm{H}}^{\mathrm{NB}}, \tag{2}$$

$$\mathcal{S}_{\mathrm{H}}^{\mathrm{B}} = \{\mathrm{N^+}, \mathrm{O^+}\}, \tag{3}$$

$$\mathcal{S}_{\mathrm{H}}^{\mathrm{NB}} = \{\mathrm{N}(1-46), \mathrm{O}(1-40)\} \cup \mathcal{S}_{\mathrm{M}}, \tag{4}$$

$$\mathcal{S}_{\mathrm{M}} = \{\mathrm{N_2}(1-4), \mathrm{NO}(1-5), \mathrm{O_2}(1-5), \mathrm{N_2^+}(1-4) \\ \mathrm{NO^+}(1-5), \mathrm{O_2^+}(1-4)\}. \tag{5}$$

The coupling of the atom and molecule electronic energy levels through the different elementary processes considered in Sec. II C allows for an explicit determination of their excitation and the radiative signature of the plasma to be obtained without the use of any *a priori* assumption on their populations.

Although negative ions can be formed (e.g., O^- and O_2^-), their contribution to the kinetics can be considered negligible, as a result of their low concentration in the nozzle and in the reservoir.

Tables I and II give the spectroscopic notation for the electronic levels of the molecules considered in this work. The spectroscopic notation is introduced for later convenience. The value of energies and degeneracies of the electronic levels of atoms (N and O) and molecules (N_2, NO, O_2, N_2^+, NO^+ and O_2^+) is given in the previous publications.[5,6,10]

C. Collisional and radiative processes

In this section, the collisional and radiative processes considered in the present work are briefly discussed. The interested reader can find more detailed information in the references included in the discussion.

1. Atomic elementary processes

The kinetic mechanism comprises:

1. Excitation by electron impact.
2. Ionization by electron impact.

The N and O atoms are efficiently excited and ionized by electron impact reactions. Due to their small mass, free electrons very easily change occupation of the attached electrons of atoms. Several models exist for the related cross sections and rate coefficients. For excitation and ionization of the first three states of N and O, we have used the rate coefficients reported by Bultel *et al.*[5] For excitation and ionization of the higher electronic states, the cross sections proposed by Drawin[19] have been adopted. In view of the hypothesis made in Sec. II A on the velocity distribution function of free electrons, the rate coefficients can be expressed under an analytical form obtained by integrating the cross sections over a Maxwellian distribution function at the free electron temperature T_e. For an electronic transition from the level i to the level j (with $E_j > E_i$), the excitation rate coefficient $k^{\mathrm{ex}}_{i\to j}$ is a function of the angular quantum numbers l_i and l_j of the levels involved. Two different cases must be distinguished:

- Optically allowed transition ($l_i \neq l_j$)

$$k^{\mathrm{ex}}_{i\to j} = 4\pi v_e a_0^2 \alpha \left(\frac{E_H}{k_{\mathrm{B}} T_e}\right)^2 I_1\left(\frac{E_j - E_i}{k_{\mathrm{B}} T_e}\right), \tag{6}$$

  with $i, j \in \mathcal{S}^{\mathrm{NB}}_{\mathrm{H}}$ (it is obvious that the indices i, j can refer to the electronic levels of only one atom between N and O). In Eq. (6), the quantity $v_e = ((8k_{\mathrm{B}}T_e)/(\pi m_e))^{1/2}$ is the free electron thermal speed (with k_{B} and m_e being, respectively, the Boltzmann constant and the free electron mass), $a_0 = 0.529 \times 10^{-10}\,\mathrm{m}$ is the first Bohr radius, $E_H = 13.6\,\mathrm{eV}$ is the ionization energy of the hydrogen atom, $\alpha = 0.05$ and I_1 is a function defined as $I_1(x) = 0.63255\, x^{-1.6454} \exp(-x)$.
- Optically forbidden transition ($l_i = l_j$)

$$k^{\mathrm{ex}}_{i\to j} = 4\pi v_e a_0^2 \alpha \left(\frac{E_j - E_i}{k_{\mathrm{B}} T_e}\right)^2 I_2\left(\frac{E_j - E_i}{k_{\mathrm{B}} T_e}\right), \tag{7}$$

  with $i, j \in \mathcal{S}^{\mathrm{NB}}_{\mathrm{H}}$. The same notation as that used for Eq. (6) applies to Eq. (7). In the latter, the quantity I_2 is a function defined as $I_2(x) = 0.23933\, x^{-1.4933} \exp(-x)$.

The rate coefficients for the reverse process (electron impact de-excitation) $k^{\mathrm{ex}}_{j\to i}$ between the levels j and i (with $j > i$) are computed by means of detailed balance

$$k^{\mathrm{dex}}_{j\to i} = k^{\mathrm{ex}}_{i\to j} \frac{g_i}{g_j} \exp\left(\frac{E_j - E_i}{k_{\mathrm{B}} T_e}\right), \quad i, j \in \mathcal{S}^{\mathrm{NB}}_{\mathrm{H}}. \tag{8}$$

For the computation of the rate coefficient for ionization by electron impact from the level i, Eq. (6) is used by replacing the upper level energy E_j with the electronic energy of

TABLE I. Electronic levels of neutral molecules.

Molecule	Level	State
N_2	1	$X^1\Sigma_g^+$
	2	$A^3\Sigma_u^+$
	3	$B^3\Sigma_g$
	4	$C^3\Pi_u$
NO	1	$X^2\Pi$
	2	$A^2\Sigma^+$
	3	$B^2\Pi$
	4	$C^2\Pi$
	5	$B'^3\Delta$
O_2	1	$X^3\Sigma_g^-$
	2	$a^1\Delta_g$
	3	$b^2\Sigma_g^+$
	4	$A^3\Sigma_u^+$
	5	$B^3\Sigma_u^-$

TABLE II. Electronic levels of charged molecules.

Molecule	Level	State
N_2^+	1	$X^2\Sigma_g^+$
	2	$A^2\Pi_u$
	3	$B^2\Sigma_u^+$
	4	$C^2\Sigma_u^+$
NO^+	1	$X^1\Sigma^+$
	2	$a^3\Sigma_+$
	3	$b^3\Pi$
	4	$b'^3\Sigma^-$
	5	$A^1\Pi$
O_2^+	1	$X^2\Pi^g$
	2	$a^4\Pi_u$
	3	$A^2\Pi_u$
	4	$b^4\Sigma_g^-$

the ground state of the ion related to that of the ground state of the atom. The rate coefficients for the reverse process (three-body recombination) are always computed by means of detailed balance.

2. Molecular elementary processes

The kinetic mechanism comprises:

1. Excitation by electron impact.
2. Ionization and dissociation by electron impact.
3. Dissociation by heavy-particle impact.
4. Dissociative recombination (and related associative ionization).
5. Exchange reactions (including Zel'dovich reactions).

The rate coefficients for excitation, ionization, and dissociation of molecular species by electron impact have been calculated by Teulet[20] and have been used in the present work. The cross section for excitation of molecules under molecular or atomic impact behaves approximately as Lotz.[21] Therefore, this form has been adopted, except when experimental data exist. In this case, the rate coefficients compiled by Teulet,[22] Capitelli,[23] and Kossyi[24] have been chosen.

The rate coefficients for the molecular dissociation by heavy-particle impact have been computed by means of the multi-temperature model of Park *et al.*[25] in order to be consistent with hypothesis made in Sec. II A regarding the population of vibrational levels of molecular species. According to the Park model, the rate coefficient for molecular dissociation by heavy-particle impact is evaluated at the average temperature $(TT_m^{\mathrm{v}})^{1/2}$, with m being the index of the molecule undergoing dissociation.

The dissociative recombination of the molecular ions is well known to play a very important role in the case of recombining plasmas. In addition, the inverse process, the associative ionization, allows in many cases for the formation of the first electrons in shock tubes, as well as in reentry problems, and consequently explains the ionizing situations. In our case, since N^+, O^+, NO^+ are present in the plasma described here, dissociative recombination has to be considered. For more details, the interested reader is referred to Bultel *et al.*[5]

Among the exchange reactions, Zel'dovich reactions can significantly influence the distribution of nitrogen and oxygen between atomic and molecular systems and can contribute to the destruction of O_2 and N_2 and formation of NO. Bose and Candler[26,27] have updated the rate coefficients for these reactions using a quasi classical trajectory (QCT) method performed starting from an *ab initio* potential energy surface calculations. Their proposed rate coefficients have been chosen for this work.

3. Radiative processes

In the present work, only bound-bound transitions are accounted for. The effect of bound-free and free-free radiative transitions is neglected.

The radiative signature of ionized air is mainly due to the spontaneous emission of the N and O atoms. Since the CR model in use is based on grouping elementary levels having similar characteristics,[5] the equivalent spontaneous emission probability of each level has to be determined. Related data are taken from the NIST database and given in Bultel *et al.*[5] In total, the number of spontaneous emission lines for N and O are 45 and 24, respectively.

As far as the molecules are concerned, some states of species mentioned in Tables I and II radiate strongly. The $\beta(B^2\Pi \rightarrow X^2\Pi)$ and $\gamma(A^2\Sigma^+ \rightarrow X^2\Pi)$ systems of NO as well as the first positive $(B^3\Pi_g \rightarrow A^3\Sigma_u^+)$ and the second positive systems $(C^3\Pi_u \rightarrow B^3\Pi_g)$ of N_2 and the first negative system $(B^2\Sigma_u^+ \rightarrow X^2\Sigma_g^+)$ of N_2^+ have been considered. The equivalent transition probability for the latter systems has been calculated fitting the data by Laux and Kruger.[28]

As stated in Sec. II A, no attempt is made in the present work in obtaining a coupled solution of the radiative transfer and nozzle flow governing equations. The possible reabsorption of radiation is estimated making use of a global escape factor α^{esc}. In what follows, it is assumed that a medium optically thin is associated to an escape factor equal to 1, whereas for an optically thick medium the escape factor is set to 0.

D. Thermodynamics

The mixture density is obtained by summing the contributions of the free electrons and the heavy-particles

$$\rho = \rho_e + \sum_{i \in \mathcal{S}_{\mathrm{H}}} \rho_i, \tag{9}$$

with ρ_e and ρ_i being, respectively, the partial density of the free electrons and the heavy-particle species i. The mixture pressure follows from the application of Dalton's law of partial pressures (where thermal non-equilibrium between the free electrons and the translation of heavy-particles must be accounted for)

$$p = \rho_e R_e T_e + \sum_{i \in \mathcal{S}_{\mathrm{H}}} \rho_i R_i T. \tag{10}$$

In Eq. (10), the quantities R_e and R_i are the specific gas constants of the free electron and the heavy-particle species i, respectively. The mixture total energy density is obtained by summing the kinetic energy density ($\rho u^2/2$, with u being the flow velocity) and the thermal energy density of all species

$$\rho E = \frac{\rho u^2}{2} + \rho_e e_e^{\mathrm{tr}}(T_e) + \sum_{i \in \mathcal{S}_{\mathrm{H}}} \rho_i [e_i^{\mathrm{tr}}(T) + \Delta h_i^{\mathrm{f}}] + \sum_{i \in \mathcal{S}_{\mathrm{H}}^{\mathrm{NB}}} \rho_i e_i + \sum_{i \in \mathcal{S}_{\mathrm{H}}^{\mathrm{B}}} \rho_i e_i^{\mathrm{el}}(T_e) + \sum_{m \in \mathcal{S}_{\mathrm{M}}} \rho_m [e_m^{\mathrm{r}}(T) + e_m^{\mathrm{v}}(T_m^{\mathrm{v}})], \tag{11}$$

from which the total enthalpy density ρH can be obtained by adding the pressure, $\rho H = \rho E + p$. In Eq. (11), the quantities $e_i^{\mathrm{tr}}(T)$ and Δh_i^{f} are, respectively, the specific translational energy and formation enthalpy of the species i (free electron, atom or molecule), while the quantities $e_m^{\mathrm{r}}(T)$ and $e_m^{\mathrm{v}}(T)$ stand for the specific rotational and vibrational energies of the molecule m. In the same equation, the quantity $e_i^{\mathrm{el}}(T)$ represents the electronic energy of the species i in the set $\mathcal{S}_{\mathrm{H}}^{\mathrm{B}}$ (whose

electronic levels are not treated as pseudo-species), while e_i represent the electronic energy of the species i in the set $\mathcal{S}_{\mathrm{H}}^{\mathrm{NB}}$.

For the computation of the specific translational and rotational energies in Eq. (11), the classical expressions obtained from the application of the principle of equipartition of energy can be employed. [The expressions given in Eqs. (12)–(14) can also be obtained by applying a classical limiting process to the discrete spectrum of energy values obtained for the particle in a box and rigid rotor quantum systems, respectively[2]]

$$e_i^{\mathrm{tr}}(T) = \frac{3}{2} R_i T, \quad i \in \mathcal{S}_{\mathrm{H}}, \tag{12}$$

$$e_e^{\mathrm{tr}}(T_e) = \frac{3}{2} R_e T_e, \tag{13}$$

$$e_m^{\mathrm{r}}(T) = R_m T, \quad m \in \mathcal{S}_{\mathrm{M}}. \tag{14}$$

Quantum effects must be considered for the evaluation of the specific vibrational energy of a molecule m. In the present work, the result obtained by using the quantum harmonic oscillator model for describing the vibration of diatomic molecule is used[2]

$$e_m^{\mathrm{v}}(T_m^{\mathrm{v}}) = \frac{R_m \theta_m^{\mathrm{v}}}{\exp(\theta_m^{\mathrm{v}}/T_m^{\mathrm{v}}) - 1}, \quad m \in \mathcal{S}_{\mathrm{M}}. \tag{15}$$

In Eq. (15), the quantity θ_m^{v} represents the characteristic temperature of vibration of the molecule m.

The expression for the electronic energy $e_i^{\mathrm{el}}(T)$ in Eq. (11) readily follows from the hypothesis of electronic levels populated according to a Boltzmann distribution

$$e_i^{\mathrm{el}}(T_e) = \frac{\sum_{l \in \mathcal{N}_i^{\mathrm{el}}} g_{il}^{\mathrm{el}}\, e_{il}^{\mathrm{el}} \exp(-\theta_{il}^{\mathrm{el}}/T_e)}{\sum_{l \in \mathcal{N}_i^{\mathrm{el}}} g_{il}^{\mathrm{el}} \exp(-\theta_{il}^{\mathrm{el}}/T_e)}, \quad i \in \mathcal{S}_{\mathrm{H}}^{\mathrm{B}}. \tag{16}$$

In Eq. (16), $\mathcal{N}_i^{\mathrm{el}}$ is the set of electronic energy levels of the species i belonging to the set $\mathcal{S}_{\mathrm{H}}^{\mathrm{B}}$. In the same equation, the quantities g_{il}^{el}, e_{il}^{el}, and $\theta_{il}^{\mathrm{el}}$ stand, respectively, for the degeneracy, the specific energy, and the characteristic temperature of the electronic energy level l belonging to the set $\mathcal{N}_i^{\mathrm{el}}$.

The thermodynamic description of the plasma is completed by specifying in Eq. (11) the numerical values of the energy (e_i) of the electronic levels treated as pseudo-species and belonging to the set $\mathcal{S}_{\mathrm{H}}^{\mathrm{NB}}$. For sake of completeness, it has to be said that also the degeneracies g_i associated to the energy levels e_i must be provided (though they do not appear explicitly in Eq. (11)).

Numerical values for the energies and degeneracies of the electronic levels treated as pseudo-species (e_i and g_i, respectively) have been taken from Bultel *et al.*,[5] while Gurvich tables[29] have been used for the remaining thermodynamic data.

E. Net volumetric mass and energy production rates

The presence of chemical and thermal non-equilibrium in a flow leads to the existence of net production rates for the mass density of each species and internal energy modes (such as molecular vibration). Energy losses due radiative transitions have also to be taken into account.

The net mass production rate ω_i for the species i expresses the time rate of change of its density due to all the collisional and radiative processes listed in Sec. II C. Its expression can be obtained from the Kinetic Theory of Gases[30]

$$\omega_i = M_i \sum_{r \in \mathcal{S}_{\mathrm{CR}}} \omega_i^r, \quad i \in \mathcal{S}, \tag{17}$$

where the quantity M_i is the molar mass of the species i and ω_i^r is the net production rate of moles of the species i due to the process r

$$\omega_i^r = \nu_i^r \left(k_r^{\mathrm{b}} \prod_{j \in \mathcal{S}} [X]_j - k_r^{\mathrm{f}} \prod_{j \in \mathcal{S}} [X]_j \right), \quad i \in \mathcal{S},\ r \in \mathcal{S}_{\mathrm{CR}}. \tag{18}$$

In Eq. (18), k_r^{f} and k_r^{b} are, respectively, the forward and backward rate coefficients for the process r, ν_i^r is the net stoichiometric coefficient of the species i for the process r, and $[X]_j$ is the concentration of the species j.

Volumetric energy production rates must be computed for the vibrational energy of molecules and the translational energy of free electrons in order to account for thermal non-equilibrium between translation of heavy-particles, free electrons and vibration of molecules, and the presence of electron impact induced processes (such as excitation, ionization, and molecular dissociation) altering the free electron energy balance. Moreover, one has to take into account for the net production rate of electronic energy of those species belonging to the set $\mathcal{S}_{\mathrm{H}}^{\mathrm{B}}$ having their electronic levels in thermal equilibrium with the free electrons (the atomic ions N^+ and O^+, see Sec. II A).

The net volumetric production rate of vibrational energy Ω_m^{v} for the molecule m is

$$\Omega_m^{\mathrm{v}} = \Omega_m^{\mathrm{VT}} + \Omega_m^{\mathrm{VV}} + \Omega_m^{\mathrm{VE}} + \Omega_m^{\mathrm{CV}}, \quad m \in \mathcal{S}_{\mathrm{M}}. \tag{19}$$

In Eq. (19), the terms Ω_m^{VT}, Ω_m^{VV}, and Ω_m^{VE} represents, respectively, the effect of inelastic collisional VT (vibration-translation), VV (vibration-vibration), and VE (vibration-electron) energy transfer processes. In the same equation, the quantity Ω_m^{CV} is the vibration-chemistry coupling term representing the net production rate of vibrational energy of the molecule m due to dissociation/recombination reactions. The VT energy transfer term Ω_m^{VT} in Eq. (19) is computed by means of the Landau-Teller model[3]

$$\Omega_m^{\mathrm{VT}} = \rho_m \frac{e_m^{\mathrm{v}}(T) - e_m^{\mathrm{v}}(T_m^{\mathrm{v}})}{\tau_m^{\mathrm{VT}}(T)}, \quad m \in \mathcal{S}_{\mathrm{M}}, \tag{20}$$

where the average relaxation time for VT transfer τ_m^{VT} is computed based on a frequency average

$$\tau_m^{\mathrm{VT}}(T) = \frac{\sum_{i \in \mathcal{S}_{\mathrm{H}}} (\rho_i / M_i)}{\sum_{i \in \mathcal{S}_{\mathrm{H}}} (\rho_i / (M_i \tau_{mi}^{\mathrm{VT}}))}, \quad m \in \mathcal{S}_{\mathrm{M}}, \tag{21}$$

with τ_{mi}^{VT} being the relaxation time for the VT interaction between the heavy-particles i and m. The latter is computed by means of Millikan and White's formula.[3] For the evaluation of the VV energy transfer term Ω_m^{VV} in Eq. (19), the model proposed by Candler[31] and modified by Knab[32] has been used

$$\Omega_m^{\mathrm{VV}} = \rho_m \sum_{l\in\mathcal{S}_{\mathrm{M}}} N_{\mathrm{A}}\sigma_{ml}P_{ml}\sqrt{\frac{8k_{\mathrm{B}}T}{\pi\mu_{ml}}}\frac{\rho_l}{m_l} \times \left(\frac{e_l^{\mathrm{v}}(T_l^{\mathrm{v}})}{e_l^{\mathrm{v}}(T)}e_m^{\mathrm{v}}(T) - e_m^{\mathrm{v}}(T_m^{\mathrm{v}})\right), \quad m\in\mathcal{S}_{\mathrm{M}}. \tag{22}$$

In Eq. (22), the quantities P_{ml} and σ_{ml} are, respectively, the exchange probability and the elastic cross-section for ml encounters (set to 10^{-2} and $1\times10^{-20}\,\mathrm{m}^2$, respectively, as suggested by Candler *et al.*[31]) m_l is the mass of the molecule l, $\mu_{ml} = m_l m_m/(m_l+m_m)$ is the reduced mass of the molecules m and l, and N_{A} is Avogadro's number. The VE energy transfer term Ω_m^{VE} in Eq. (19) is computed by means a model similar to that used for the VT transfer (Eq. (20))

$$\Omega_m^{\mathrm{VE}} = \rho_m \frac{e_m^{\mathrm{v}}(T_e) - e_m^{\mathrm{v}}(T_m^{\mathrm{v}})}{\tau_m^{\mathrm{VE}}(T_e)}, \quad m\in\mathcal{S}_{\mathrm{M}}. \tag{23}$$

The formula for the relaxation time τ_m^{VE} is taken from the work of Bourdon *et al.*[33] in the case of the N_2 molecule. For other molecules (such as NO and O_2), the VE process is not considered since the energy transfer process is much less efficient.[3] For the evaluation of the net volumetric production rate of vibrational energy Ω_m^{CV} of the molecule m due to dissociation/recombination reactions in Eq. (19), the non-preferential-dissociation model proposed by Candler[31] has been considered

$$\Omega_m^{\mathrm{CV}} = \omega_m e_m^{\mathrm{v}}(T_m^{\mathrm{v}}), \quad m\in\mathcal{S}_{\mathrm{M}}. \tag{24}$$

According to Eq. (24), the average vibrational energy lost/gained by the molecule m due to dissociation/recombination reactions is equal to the bulk vibrational energy of the molecule m. This constitutes an approximation, as molecules tend to dissociate/recombine preferentially in high-lying vibrational states.[9,13,18,34–36] Macheret *et al.*[34] have proposed a model (within the context of a multi-temperature description of thermal non-equilibrium) in order to account for the preferential nature of molecular dissociation/recombination by heavy-particle impact. However, as it is shown in Sec. V E, the differences between the results obtained by using Macheret's model[34] and the non-preferential-dissociation model (Eq. (24)) are barely noticeable in our test-case.

The net volumetric production rate Ω_e for the translational energy of free electron and electronic energy of the species belonging to the set $\mathcal{S}_{\mathrm{H}}^{\mathrm{B}}$ (hence, for the portion of the gas whose thermal energy is in equilibrium at the temperature T_e) is

$$\Omega_e = \Omega^{\mathrm{TE}} + \Omega^{\mathrm{EI}} + \Omega^{\mathrm{ED}} + \Omega^{\mathrm{EE}} + \sum_{i\in\mathcal{S}_{\mathrm{H}}^{\mathrm{B}}} \omega_i e_i^{\mathrm{el}}(T_e) - \sum_{m\in\mathcal{S}_{\mathrm{M}}} \Omega_m^{\mathrm{VE}}. \tag{25}$$

In Eq. (25), the terms Ω^{TE}, Ω^{EI}, Ω^{ED}, and Ω^{EE} are, respectively, the net volumetric production rate of the free electron energy due to elastic collisions with heavy-particles, electron impact ionization, electron impact dissociation, and electron impact excitation processes. In the same equation, the fourth term $\sum_{i\in\mathcal{S}_{\mathrm{H}}^{\mathrm{B}}} \omega_i e_i^{\mathrm{el}}(T_e)$ represents the net production rate of electronic energy of the N^+ and O^+ ions, while the last one accounts for the vibration-electron energy exchange process. The effect of radiative transitions does not appear in Eq. (25), as only bound-bound transitions are considered. The elastic collision term Ω^{TE} in Eq. (25) is computed according to

$$\Omega^{\mathrm{TE}} = \frac{3}{2}n_e k_{\mathrm{B}}(T-T_e)\sum_{i\in\mathcal{S}_{\mathrm{H}}} 2\left(\frac{m_e}{m_i}\right)\nu_e n_i \bar{\Omega}_{ei}^{(1,1)}, \tag{26}$$

where n_e and n_i are, respectively, the number density of the free electrons and the heavy-particle i, while $\bar{\Omega}_{ei}^{(1,1)}$ is the electron-heavy (1, 1)-type collision integral for the elastic interaction between the aforementioned species.[37] The evaluation of the terms Ω^{EI}, Ω^{ED}, and Ω^{EE} associated to electron impact ionization, dissociation, and excitation in Eq. (25) has been performed as follows. If one considers, as an example, an excitation process between the levels i and j (with $E_j > E_i$), the energy lost by the free electron ΔE can be computed from the energy balance for the collisional event. Since in collisions between free electrons and heavy-particles, the velocity of the latter does not change significantly due to the large mass disparity, the energy balance can be written as

$$\frac{1}{2}m_e v^2 + E_i = \frac{1}{2}m_e v'^2 + E_j, \quad i,j\in\mathcal{S}_{\mathrm{H}}^{\mathrm{NB}} \tag{27}$$

where the quantities v and v' are the free electron pre- and post-collisional velocities. From Eq. (27), one readily obtains the energy lost by the free electron ΔE

$$\Delta E = \frac{1}{2}m_e v'^2 - \frac{1}{2}m_e v^2 = E_j - E_i, \quad i,j\in\mathcal{S}_{\mathrm{H}}^{\mathrm{NB}}. \tag{28}$$

The net volumetric production rate of free electron energy due to the electron impact process leading to the transition $i\rightarrow j$ (with $E_j > E_i$) is then

$$-M_i\,\omega_{i\rightarrow j}^{\mathrm{ex}}(e_j - e_i), \quad i,j,\in\mathcal{S}_{\mathrm{H}}^{\mathrm{NB}}, \quad (e_j > e_i), \tag{29}$$

where the minus sign is used since the energy is lost by the free electron. In Eq. (29), the molar production term $\omega_{i\rightarrow j}^{\mathrm{ex}}$ is computed from the general formula given in Eq. (18) and the energies of the electronic levels involved have been expressed as specific energies in order to obtain a net volumetric energy production rate with the units of a power per unit volume ($\mathrm{W/m^3}$). The sum of Eq. (29) over all the electron impact excitation processes gives the term Ω^{EE} in Eq. (25). As already mentioned before (see Eq. (6)), it is obvious that the indices i and j in Eq. (29) refer to two electronic levels belonging to only one atomic or molecular species. A similar approach can be used for the electron impact dissociation and ionization processes for computing the terms Ω^{EI}

and Ω^{ED} in Eq. (25), by replacing the energy of the upper level E_j with the dissociation/ionization energy of the species involved (a rigorous approach, based on Kinetic Theory, for computing the term Ω^{EI} can be found in Magin *et al.*[38]).

The last net volumetric energy production rate to be accounted for is that due to bound-bound radiative transitions Q^{rad}. The former is expressed as

$$Q^{rad} = \alpha^{esc} \sum_{\substack{i,j \in \mathcal{S}_H^{NB}, \\ E_j < E_i}} A_{ij} n_i (E_i - E_j) + \alpha^{esc} \sum_{\substack{i,j \in \mathcal{S}_H^{NB}, \\ E_j > E_i}} A_{ij} n_i (E_j - E_i), \tag{30}$$

where α^{esc} is the escape factor (introduced to account for possible radiation re-absorption) and A_{ij} is the Einstein coefficient for the spontaneous emission associated to the radiative transition between the levels i and j. The same discussion of before, regarding the energy level indices i and j, applies to Eq. (30).

III. GOVERNING EQUATIONS

The governing equations for the inviscid and quasi-one-dimensional non-equilibrium flow through a nozzle of given cross sectional area distribution $A = A(x)$ can be written in conservation law form as

$$\frac{\partial \mathbf{U}}{\partial t} + \frac{\partial \mathbf{F}}{\partial x} = \mathbf{S}, \tag{31}$$

where $\mathbf{U}$, $\mathbf{F}$, and $\mathbf{S}$ are the conservative, inviscid flux, and source term vectors, respectively. The source term vector $\mathbf{S}$ in Eq. (31) can be written as

$$\mathbf{S} = \mathbf{\Omega} - \frac{d \ln A}{dx} \mathbf{G}. \tag{32}$$

In Eq. (32), the vector $\mathbf{\Omega}$ represents the effects of collisional and radiative processes previously described, while the vector $-d \ln A/dx\, \mathbf{G}$ accounts for the nozzle cross sectional area variation. After introducing the quantity $\rho e^{e-el}(T_e)$, representing the portion of the gas whose thermal energy density is in equilibrium at the temperature T_e and which is defined as

$$\rho e^{e-el}(T_e) = \rho_e e_e^{tr}(T_e) + \sum_{i \in \mathcal{S}_H^B} \rho_i e_i^{el}(T_e), \tag{33}$$

the expressions for the vectors $\mathbf{U}$, $\mathbf{F}$, $\mathbf{G}$, and $\mathbf{\Omega}$ in Eqs. (31) and (32) are

$$\mathbf{U} = [\, \rho_i \quad \rho u \quad \rho E \quad \rho_m e_m^v \quad \rho e^{e-el} \,]^T, \tag{34}$$

$$\mathbf{F} = [\, \rho_i u \quad p + \rho u^2 \quad \rho u H \quad \rho_m e_m^v u \quad \rho e^{e-el} u \,]^T, \tag{35}$$

$$\mathbf{G} = [\, \rho_i u \quad \rho u^2 \quad \rho u H \quad \rho_m e_m^v u \quad \rho e^{e-el} u \,]^T, \tag{36}$$

$$\mathbf{\Omega} = [\, \omega_i \quad 0 \quad -Q^{rad} \quad \Omega_m^v \quad \Omega_e - p_e \partial u/\partial x \,]^T, \tag{37}$$

with $i \in \mathcal{S}$ and $m \in \mathcal{S}_M$. In Eqs. (34)–(37), the explicit functional dependence on the temperatures of the quantities involved (such as $\rho_m e_m^v(T_m^v)$ and $\rho e^{e-el}(T_e)$) has been dropped for sake of clarity.

IV. NUMERICAL METHOD

Numerical solutions of the governing equations are obtained as follows. The finite volume method is applied for the discretization of Eq. (31), leading to the following ordinary differential equation describing the time evolution of the cell i conservative variable vector $\mathbf{U}_i$

$$\frac{d\mathbf{U}_i}{dt} \Delta x_i + \tilde{\mathbf{F}}_{i+\frac{1}{2}} - \tilde{\mathbf{F}}_{i-\frac{1}{2}} = \mathbf{S}_i \Delta x_i, \tag{38}$$

with the cell volume (length) $\Delta x_i = x_{i+1/2} - x_{i-1/2}$. The numerical flux $\tilde{\mathbf{F}}_{i+1/2}$ in Eq. (38) is computed by means of the AUSM (Advection Upstream Splitting Method) scheme[39] with a modified definition of the interface speed of sound.[40] In order to allow for a straightforward calculation of thermo-chemical properties, which can be computed directly from the local temperatures rather than from energies, the solution is stored in natural variables $\mathbf{P}$

$$\mathbf{P} = [\, \rho_i \quad u \quad T \quad T_m^v \quad T_e \,]^T, \quad i \in \mathcal{S},\ m \in \mathcal{S}_M. \tag{39}$$

Since the solution update is also performed in natural variables, Eq. (38) is re-written by applying the chain rule to the term $d\mathbf{U}_i/dt$

$$\frac{\partial \mathbf{U}_i}{\partial \mathbf{P}_i} \frac{d\mathbf{P}_i}{dt} \Delta x_i + \tilde{\mathbf{F}}_{i+\frac{1}{2}} - \tilde{\mathbf{F}}_{i-\frac{1}{2}} = \mathbf{S}_i \Delta x_i. \tag{40}$$

Equation (40) (written per each cell) is integrated in time by means of a standard backward Euler implicit procedure in order to march from the time level n to $n+1$. Because of the non-linear nature of the discretized set of equations (Eq. (40)), a local Newton linearization around the solution at the time level n is performed. This leads to a block tridiagonal linear algebraic system to be solved for the variation between the time levels $n+1$ and n of the natural variable vector $\delta \mathbf{P}_i^n = \mathbf{P}_i^{n+1} - \mathbf{P}_i^n$ for each cell

$$\tilde{\mathbf{A}}_i^n \delta \mathbf{P}_{i-1}^n + \tilde{\mathbf{B}}_i^n \delta \mathbf{P}_i^n + \tilde{\mathbf{C}}_i^n \delta \mathbf{P}_{i+1}^n = -\tilde{\mathbf{R}}_i^n. \tag{41}$$

The matrices $\tilde{\mathbf{A}}_i$, $\tilde{\mathbf{B}}_i$, and $\tilde{\mathbf{C}}_i$ and the right-hand-side residual $\tilde{\mathbf{R}}_i$ in Eq. (41) are

$$\tilde{\mathbf{A}}_i = -\frac{\partial \tilde{\mathbf{F}}_{i-1/2}}{\partial \mathbf{P}_{i-1}}, \tag{42}$$

$$\tilde{\mathbf{B}}_i = \left(\frac{1}{\Delta t_i} \frac{\partial \mathbf{U}_i}{\partial \mathbf{P}_i} - \frac{\partial \mathbf{S}_i}{\partial \mathbf{P}_i} \right) \Delta x_i + \frac{\partial \tilde{\mathbf{F}}_{i+1/2}}{\partial \mathbf{P}_i} - \frac{\partial \tilde{\mathbf{F}}_{i-1/2}}{\partial \mathbf{P}_i}, \tag{43}$$

$$\tilde{\mathbf{C}}_i = \frac{\partial \tilde{\mathbf{F}}_{i+1/2}}{\partial \mathbf{P}_{i+1}}, \tag{44}$$

$$\tilde{\mathbf{R}}_i = \tilde{\mathbf{F}}_{i+\frac{1}{2}} - \tilde{\mathbf{F}}_{i-\frac{1}{2}} - \mathbf{S}_i \Delta x_i. \tag{45}$$

The cell time-step Δt in Eq. (43) is computed based on the Courant-Friedrich-Lewy (CFL) number σ as $\Delta t = \sigma \Delta x / (|u| + c)$ (with c being the local frozen speed of sound).[41] The

algebraic system in Eq. (41) is assembled by evaluating the Jacobian matrices in Eqs. (42)–(44) numerically (with the exception of the transformation matrix $\partial\mathbf{U}/\partial\mathbf{P}$ that can be easily evaluated analytically). The solution for the vector $\delta\mathbf{P}$ in Eq. (41) is found iteratively by means of the GMRES algorithm[42] (together with the Incomplete-Lower-Upper (ILU) preconditioning[42]). The natural variable vector for each cell is then updated to the time level $n+1$ according to

$$\mathbf{P}_i^{n+1} = \mathbf{P}_i^n + \delta\mathbf{P}_i^n. \tag{46}$$

This process is continued until steady state is reached.

A weighted MUSCL (Monotone Upstream Centered Schemes for Conservation Laws) method[43] is applied in order to achieve second order accuracy in space. The reconstruction is performed on the vector natural variables (Eq. (39)) and limited (in steep gradient regions) by means of the van Albada limiter.[44] Boundary conditions are applied through ghost cells.[41]

V. COMPUTATIONAL RESULTS

The electronic specific CR model for ionized air described in Sec. II has been used to investigate non-equilibrium effects in the flow within the nozzle of VKI minitorch facility. Numerical solutions to the governing equations given in Sec. III have been obtained by means of the numerical method described in Sec. IV and implemented in the VKI COOLFluiD parallel framework.[40,45,46] The MUTATION library[47] (interfaced within the COOLFluiD framework) has been used for the evaluation of species thermodynamic properties and source terms due to collisional and radiative processes.

Figure 1 shows the normalized area distribution of the nozzle of the VKI minitorch facility. In all the computations shown in the present paper, the total pressure and temperature in the nozzle reservoir have been set to $p_0 = 101\,325$ Pa and $T_0 = 10\,000$ K, respectively. Local thermodynamic equilibrium (LTE) conditions have been assumed at the nozzle inlet. Preliminary computations, performed by using a different vibrational temperature for each molecular species, have shown that the vibrational temperatures of molecular ions (N_2^+, NO^+, and O_2^+) were very close to that of the N_2 molecule. In view of that, it was decided to perform all the calculations by using a unique vibrational temperature for the aforementioned molecules, that is

$$T^{\mathrm{v}}_{\mathrm{N_2}} = T^{\mathrm{v}}_{\mathrm{N_2^+}} = T^{\mathrm{v}}_{\mathrm{NO^+}} = T^{\mathrm{v}}_{\mathrm{O_2^+}}, \tag{47}$$

for which the related equation is obtained by summing together the vibrational energy conservations equation for the N_2, N_2^+, NO^+ and O_2^+ molecules (see Sec. III). With the exception of Sec. V D, all the results refer to an optically thick medium ($\alpha^{\mathrm{esc}} = 0$ in Eq. (30)).

A. Flow-field characterization

The knowledge of pressure, temperatures, and free electron number density inside the nozzle is of primary concern since it allows us to characterize important features of the physico-chemical state of the plasma.

An accurate investigation of the evolution of these flow quantities is presented here. The behavior of the pressure along the nozzle is depicted in Fig. 2. Most of the expansion in the flow takes place in the diverging part, being the pressure constant up to the throat. The pressure has a strong influence on the thermo-physical and chemical state of the plasma since it influences the response time of the gas to the changes in the thermodynamic properties occurring along the expansion. The first part of the nozzle is characterized by high pressure and low velocity and in these conditions the plasma is in equilibrium. As the flow moves downstream towards the throat and the nozzle outlet, the first non-equilibrium effects begin to appear since the pressure is low and the flow velocity is maximum. Temperature profiles are shown in Fig. 3. The vibrational temperature of the N_2 molecule and the free-electron translational temperature are strongly coupled to each other thanks to the VE energy exchange process and reach a state of partial equilibrium

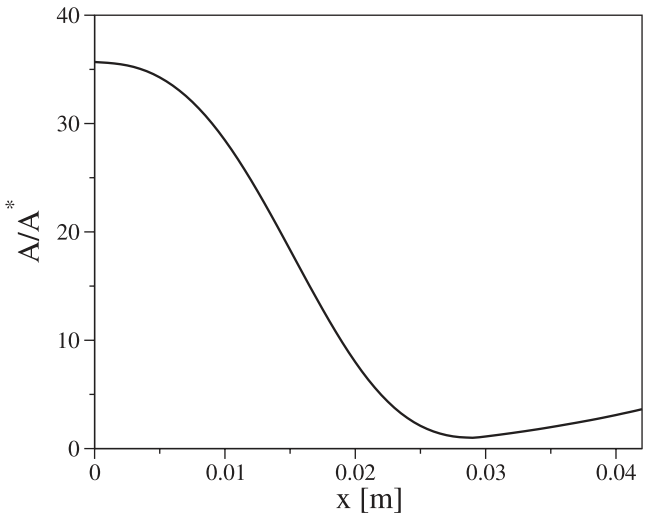

FIG. 1. Normalized area distribution of the nozzle of the VKI minitorch facility (throat at $x = 0.029$ m).

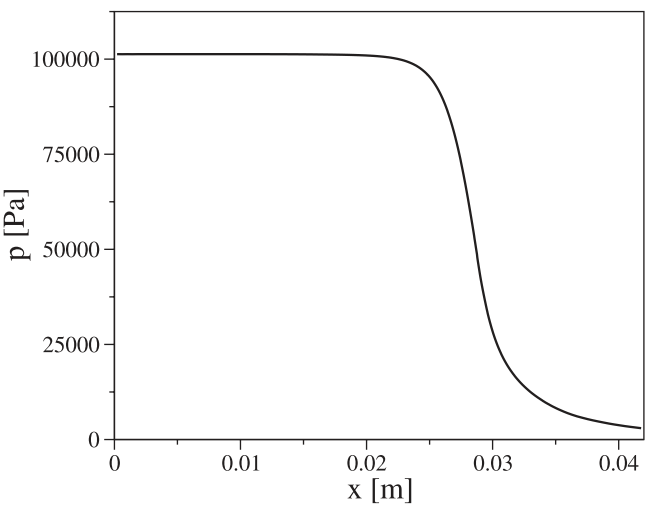

FIG. 2. Pressure evolution along the nozzle axis.

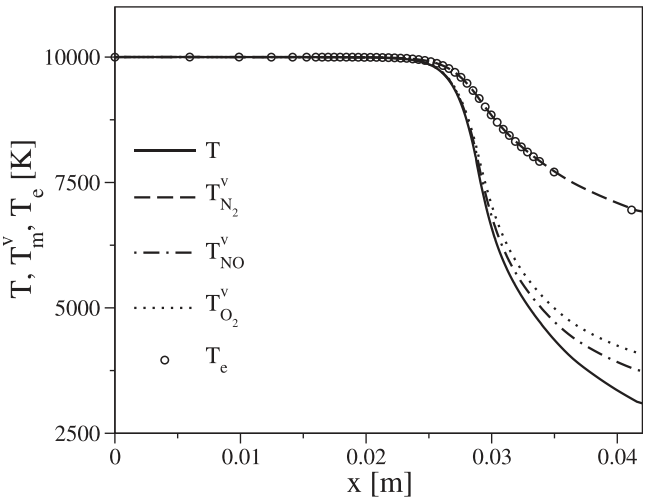

FIG. 3. Temperature evolution along the nozzle axis.

between each other in the diverging part of the nozzle. Different is the behavior of the NO and O_2 molecules, whose vibrational temperatures stay close to equilibrium values and show small departures from the translational temperature.

Table III summarizes the characteristic quantities of the flow in correspondence of the nozzle outlet, and in particular, two different values of the electron number density are indicated: n_e and n_e^{EQ}.

While the first value refers to the computed number density at the outlet, the second value represents the equilibrium number density expected at 3097 K and 2980 Pa, which are the free-electron temperature and static pressure at the nozzle outlet. A strong non-equilibrium of the free electrons density is observed, which, as it will be shown in Secs. V B and V C, causes an overpopulation of the electronic excited states of the atoms and molecules, since free electrons are very efficient as collision partner for electronic excitation.

TABLE III. Outlet conditions ($x = 0.042$ m).

T	3097 K
$T^v_{N_2}$	6922 K
T^v_{NO}	3742 K
$T^v_{O_2}$	4089 K
T_e	6893 K
n_e	1.23×10^{21} 1/m^3
n_e^{EQ}	1.57×10^{16} 1/m^3
p	2980 Pa

B. Analysis of the atomic distribution functions

The converging part of the nozzle is characterized by high values of the static pressure and the distribution of the excited states tends to follow a Boltzmann distribution. Therefore, the knowledge of pressure and temperature is sufficient to the description of physico-chemical state of the plasma. However, as the nozzle throat is approached, the gas rapidly expands and the collisional excitation may not be sufficient to maintain the equilibrium between the electronic levels of atoms and molecules. Radiative processes have also an influence on the shape of the distribution function, by means of radiative transitions.

Figure 4(a) shows the electronic distribution function of the N atom in correspondence of the nozzle throat. It is interesting to observe that at this location the population is very close to a Boltzmann distribution even if the vibrational non-equilibrium effects are already present as shown in Fig. 3. The O atom exhibits the same type of behavior (see Fig. 4(b)) in correspondence of the nozzle throat and is found to be in Boltzmann equilibrium.

Moving the focus of our analysis to the outlet of the nozzle a strong overpopulation of the excited states of the N and O atoms is observed (see Fig. 5). The same physical phenomena have been observed experimentally in argon plasmas produced by electromagnetic discharges.[48–50] The

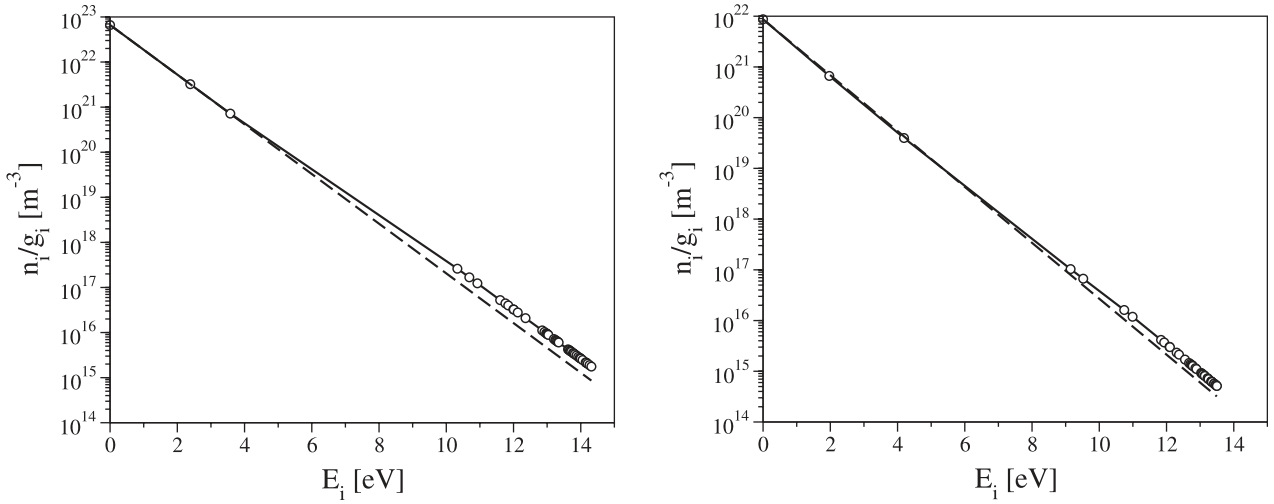

(a) N atom. (b) O atom.

FIG. 4. N and O atoms: comparison of the non-equilibrium (lines with symbols) and equilibrium (dashed lines) population distribution of the electronic levels at the nozzle throat ($x = 0.029$ m, $T_e = 9163$ K).

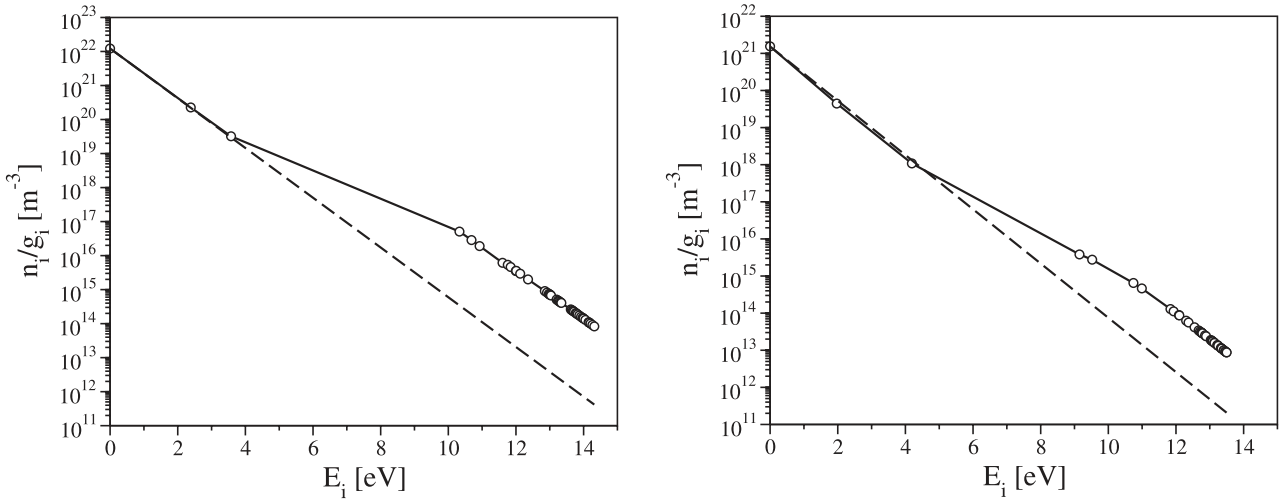

FIG. 5. N and O atoms: comparison of the non-equilibrium (lines with symbols) and equilibrium (dashed lines) population distribution of the electronic levels at the nozzle outlet ($x = 0.042$ m, $T_e = 6893$ K).

influences of the non Boltzmann distribution of the excited states on the temperature measurements is discussed by Owano *et al.*[48]

Only by accounting for the non-LTE distribution of excited states, it is possible to find agreement among spectroscopic measurements, based on the analysis of the atomic line radiation and an independent calorimetric energy balance. In molecular gases, however, those effects may be reduced for two reasons. First, in air, electrons couple strongly with the N_2 molecule vibration. Since the vibrational temperature thermalizes with the translational energy of heavy particles by means of the VT energy exchange process, as a result the translational temperature of free electrons is cooled and the ionization degree is lower. Second, the main mechanism of recombination of the free electrons is due to dissociative recombination, which is a two body process and, as such, is much faster than the three body recombination taking place in atomic plasmas.[51] The population distributions given in Fig. 5 show that, in recombining plasmas, the high-lying bound electrons tend to behave like the free electrons. This situation is completely opposite to what is found when analyzing the ionizing plasmas produced by strong shock waves. An example of that is given in Panesi *et al.*,[6] where the CR model used in the present work has been applied to investigate the non-equilibrium flow behind a normal shock wave. In the aforementioned work, it was noticed that the electronic levels of the upper states are in Saha equilibrium with the free electrons and they are not in thermal equilibrium with the ground electronic state. In recombining plasmas, the free electron density exceeds the equilibrium value (see Table III) and the overpopulation of the free electrons causes an overpopulation of the high-lying excited states.[52] This situation is opposite to the ionizing situation where the lack of free electrons, due to non-equilibrium effects, induces a depletion of the high-lying excited states.

In conclusion, the analysis of the electronic levels population of atomic species, here discussed, demonstrates the importance of the use of a state-specific approach to capture the deviation of the population of the excited electronic levels from the equilibrium distribution. If neglected, such effects may lead to a misinterpretation of the experimental results.[48]

C. Analysis of the molecular distribution functions

The analysis of the evolution of the electronic states of the molecules in a post-discharge environment is addressed in numerous contributions.[51,53–55] In general, an overpopulation of excited states occur, which is confirmed by spectroscopic measurements.[51] In this section, the population of the excited states is compared with the corresponding equilibrium values in order to analyze the thermodynamic state of the molecular species.

Figure 6 shows the behavior of the ground and the excited states of the N_2 molecule. A comparison is carried

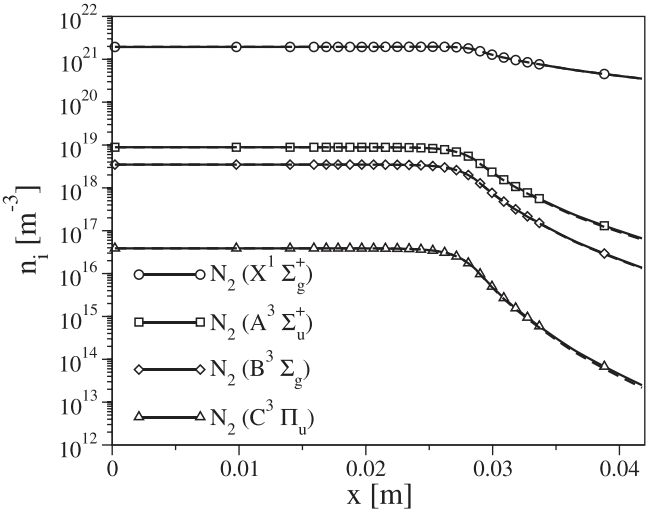

FIG. 6. N_2 molecule: comparison of the non-equilibrium (lines with symbols) and equilibrium (dashed lines) populations of the electronic levels.

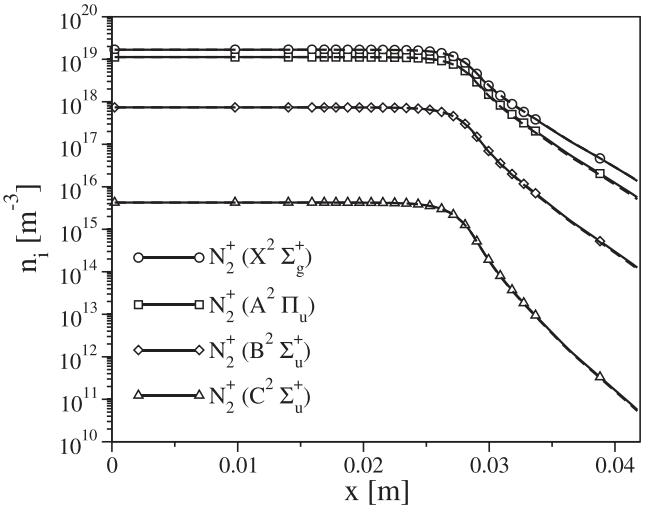

FIG. 7. N_2^+ molecule: comparison of the non-equilibrium (lines with symbols) and equilibrium (dashed lines) populations of the electronic levels.

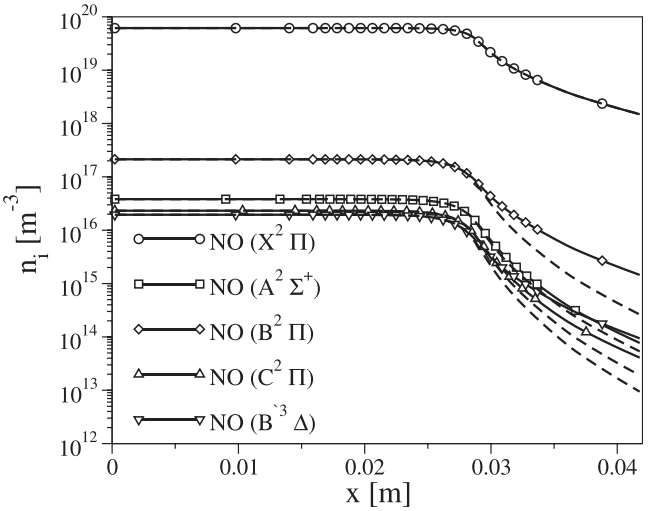

FIG. 8. NO molecule: comparison of the non-equilibrium (lines with symbols) and equilibrium (dashed lines) populations of the electronic levels.

out with the corresponding equilibrium values at each location along the nozzle axis. Equilibrium calculations (dashed lines) have been carried out extracting number density and temperatures of the individual molecule under analysis assuming that the excited states are populated according to a Boltzmann distribution.

The figure shows that the population of the N_2 molecule, which is supposed to be in equilibrium in the reservoir, stays in equilibrium throughout all the expansion although a slight overpopulation of the $C^3\Pi_u$ state is present. Similar behavior can be observed for the excited states of N_2^+ molecule in Fig. 7 where the overpopulation of the $B^2\Sigma_u^+$ state is very small. The excitation processes of the $B^2\Sigma_u^+$ state of the N_2^+ molecule are modeled using rate constants estimated by Teulet.[22] However, a comparison of those rates with others found in literature[56] shows large discrepancies. Therefore, the conclusions concerning the state of degree of non-equilibrium of the N_2^+ molecule may strongly depend on the model used for the kinetic processes.

Different is the behavior of the NO, NO^+, and O_2 molecules which are found to depart from equilibrium in proximity of the nozzle outlet. In Fig. 8, the population of exited states of the NO molecule are found to be overpopulated by one order of magnitude, with a consequent enhancement of the radiative signature through the $\beta(B^2\Pi \rightarrow X^2\Pi)$ and $\gamma(A^2\Sigma \rightarrow X^2\Pi)$ systems. Similar is the behavior of the NO^+ and O_2 molecules (not shown here) where the excited states follow the same trend of the NO molecule.

The foregoing analysis leads to the conclusion that the population of the N_2 and N_2^+ molecules can be described by a Boltzmann distribution at the free electron temperature T_e. Different is the behavior of the other molecular species which are found strongly overpopulated in correspondence of the nozzle outlet.

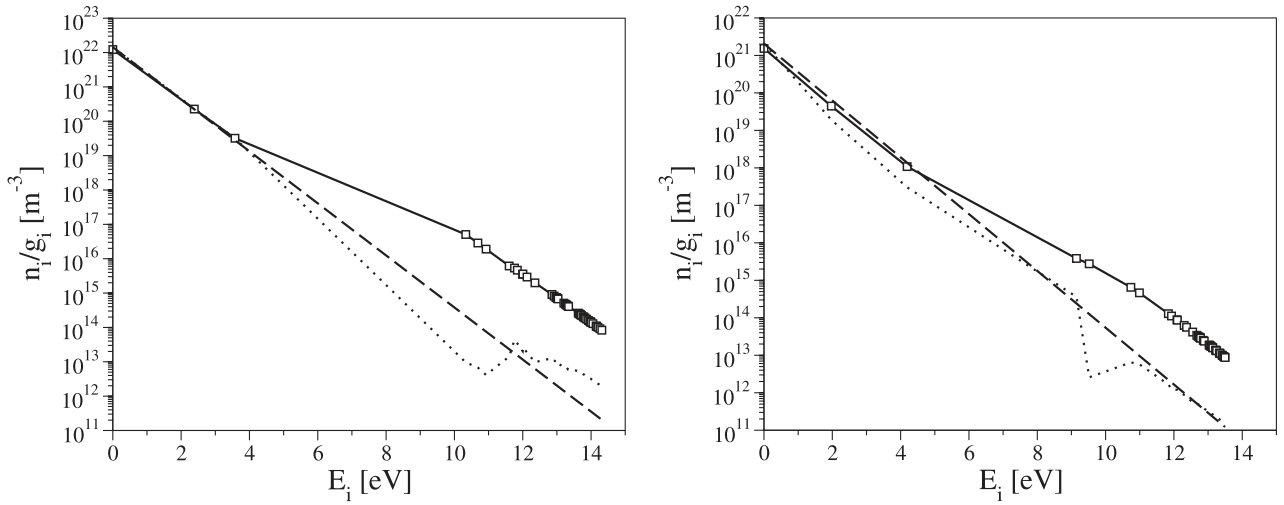

(a) N atom. (b) O atom.

FIG. 9. N and O atoms: population distribution of the electronic levels at the nozzle outlet in the case of optically thick (lines with symbols) and optically thin medium (dotted lines). The dashed lines indicate the equilibrium population distributions for the optically thick medium case.

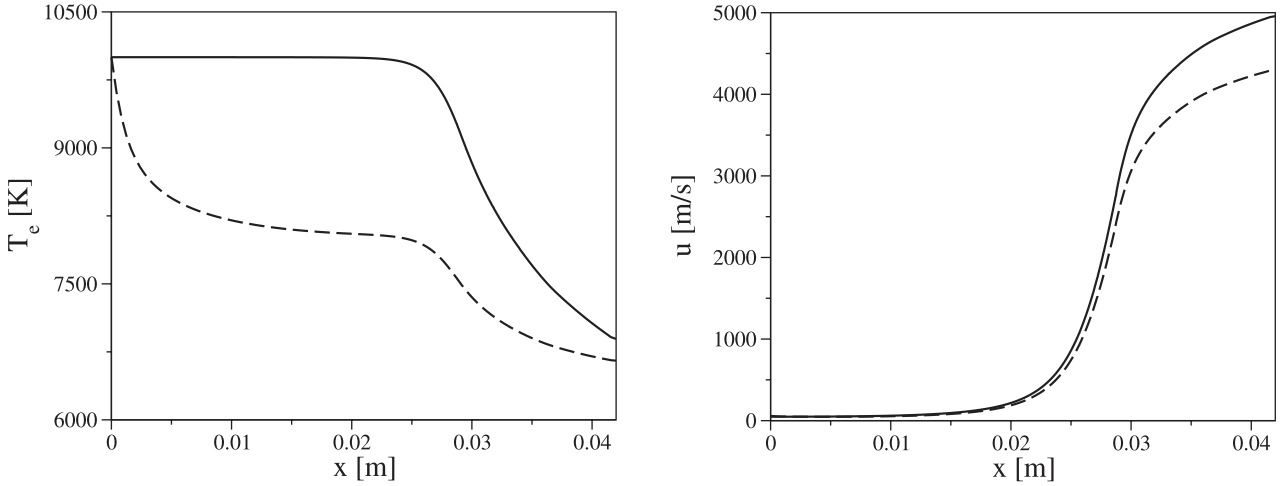

(a) Free electron temperature. (b) Velocity.

FIG. 10. Comparison of the free-electron temperature and velocity for the case of optically thick (lines) and optically thin medium (dashed lines).

D. Influence of radiative losses

After the analysis of the nozzle flow-field and atomic and molecular distribution functions in the case of an optically thick medium (Secs. V A and V B), the effects of radiative losses have been studied for the case of an optically thin medium by setting $\alpha^{esc} = 1$ in Eq. (30).

The effects of the radiative transitions on the population of the electronic states of the N and O atoms can be observed in Fig. 9. In the same figure, the population distribution obtained for the case of an optically thick medium ($\alpha^{esc} = 0$) are also shown for sake of clarity. The resonance lines tend to deplete the excited levels and for some states the population is below the Boltzmann prediction. The high-lying levels are very closely coupled by kinetic processes, and the depletion of the emitting levels affects the general behavior of the neighbor levels and, as a consequence, all the population is lowered. Moreover, being the expansion not adiabatic due to the energy losses, the free electrons cool down and contribute to a general reduction of the electronic excitation degree.

Radiative transitions have effects also on macroscopic quantities, as can be appreciated from Fig. 10 showing a comparison for the free electron temperature and the flow velocity in the case of optically thin and thick medium.

E. Influence of the vibration-chemistry coupling

In order to assess the approximation introduced by the use of the non-preferential-dissociation model (see Sec. II E) for the evaluation of the average energy gained/lost by molecules due to dissociation/recombination reactions by heavy-particle impact, the calculations presented in Secs. V A–V C have been repeated by using the preferential-dissociation model proposed by Macheret *et al.*[34]

Figure 11 shows the evolution along the nozzle axis of the N_2 molecule mass fraction. The global amount of recombination is very small, with Candler's model providing a slightly higher value of the N_2 molecule mass fraction at the nozzle outlet. The same conclusion holds for the other molecular species and for macroscopic flow quantities such as velocity and temperatures (not shown here). The use of a preferential-dissociation model does not lead to appreciable differences even when looking at microscopic quantities such as the molecular distribution functions. Figure 12 shows the comparison for the N_2 and NO molecules. The curves obtained by means of Candler and Macheret's models simply overlap.

The good agreement shown in previous pictures is not surprising for the following reasons:

- The global amount of recombination is very small. The former is strongly influenced by the nozzle shape.[1] In the present work, the nozzle geometry in use (see Fig. 1) has a diverging portion which is shorter than the converging one and an inlet/outlet area ratio bigger than one. Based on that, a small amount of recombination should be expected.

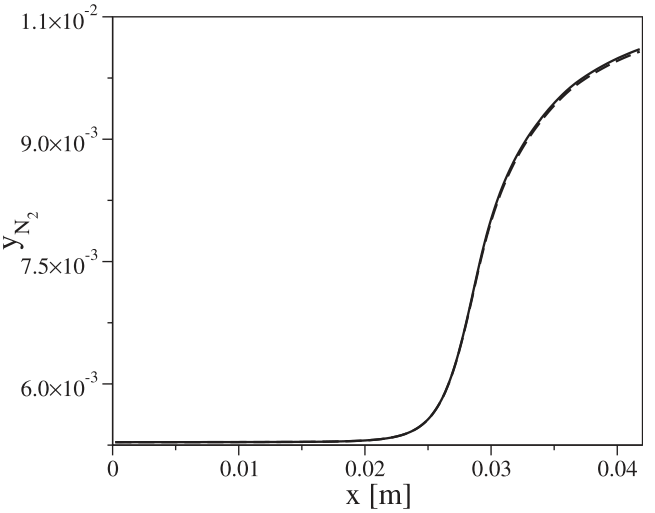

FIG. 11. N_2 molecule: comparison of the mass fraction for Candler (lines) and Macheret's (dashed lines) models for chemistry-vibration coupling.

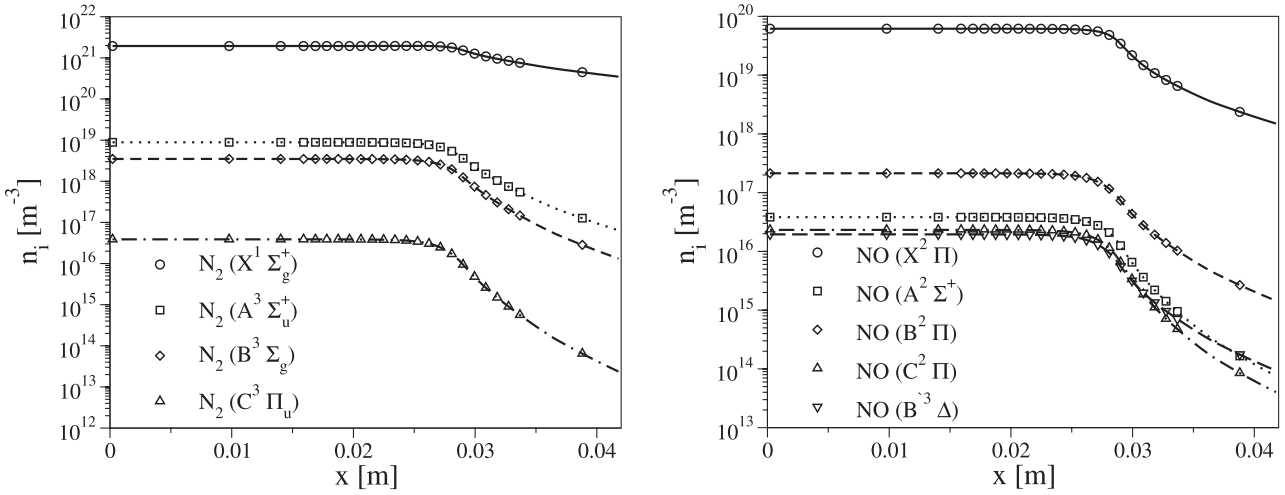

(a) N_2 molecule. (b) NO molecule.

FIG. 12. N_2 and NO molecules: comparison of the non-equilibrium populations of the electronic levels for Candler (symbols) and Macheret's (lines) models for chemistry-vibration coupling.

- One of the main channel for molecular recombination within plasma flows analyzed in the present work is the dissociative recombination of molecular ions (not taken into account in Macheret's model).

From the previous discussion, one can conclude that the use of the non-preferential-dissociation model is justified for the calculations shown in the present work.

VI. CONCLUSIONS

An existing electronically specific Collisional-Radiative model has been used to study the behavior of atomic and molecular excited levels in the non-equilibrium plasma inside the nozzle of the Minitorch facility at the von Karman Institute. The effects of radiative losses have been accounted for by means of escape factors. The results clearly show that the optical thickness of the plasma has a strong influence on the dynamics of the electronic levels of atoms and molecules.

- For the optically thick case, a strong overpopulation of high-lying electronic levels has been observed for all the chemical components, with the exception of the N_2 and N_2^+ molecules. The population of the electronic levels of N_2 and N_2^+ were found in Boltzmann equilibrium at the free electron temperature.
- When the medium is considered optically thin, the overpopulation of the excited states of the N and O atoms is drastically reduced.

Future work will focus on:

- Implementation of a more physically consistent model based on the self-consistent coupling of radiation and flow-field, discussed in detail by Huo *et al.*[17]
- Continue the validation process of the electronic specific CR model in use (already performed for compressing flows behind shock waves[16]) by means of comparison with spectroscopic measurements in expanding flows.

ACKNOWLEDGMENTS

The authors have benefited from numerous discussions with Dr. A. Bourdon at the EM2C Laboratory at Ecole Centrale Paris and Professor T. E. Magin at the von Karman Institute for Fluid Dynamics.

[1]J. D. Anderson, *Hypersonic and High Temperature Gas Dynamics* (McGraw-Hill, New York, 1989).
[2]W. J. Vincenti and C. H. Kruger, *Introduction to Physical Gas Dynamics* (Wiley, New York, 1965).
[3]C. Park, *Nonequilibrium Hypersonic Aerothermodynamics* (Wiley, New York, 1990).
[4]C. Park, "The limits of two temperature model," AIAA Paper 2010–911, 2010.
[5]A. Bultel, B. G. Chéron, A. Bourdon, O. Motapon, and I. F. Schneider, "Collisional-radiative model in air for earth re-entry problems," Phys. Plasmas **13**, 043502 (2006).
[6]M. Panesi, T. E. Magin, A. Bourdon, A. Bultel, and O. Chazot, "Analysis of the Fire II flight experiment by means of a collisional-radiative model," J. Thermophys. Heat Transfer **23**, 236–248 (2009).
[7]F. Esposito and M. Capitelli, "Quasi-classical molecular dynamic calculations of vibrationally and rotationally state selected dissociation cross sections: $N + N_2 \rightarrow 3N$," Chem. Phys. Lett. **302**, 49–54 (1999).
[8]F. Esposito and M. Capitelli, "Quasi-classical dynamics and vibrational kinetics of $N + N_2(v)$ system," Chem. Phys. **257**, 193–202 (2000).
[9]G. Colonna and M. Capitelli, "Self-consistent model of chemical, vibrational, electron kinetics in nozzle expansion," J. Thermophys. Heat Transfer **15**, 308–316 (2001).
[10]M. Panesi, T. Magin, A. Bourdon, A. Bultel, and O. Chazot, "Study of electronically excited state populations of atoms and molecules predicted by means of a collisional-radiative model for the Fire II flight experiment," J. Thermophys. Heat Transfer **25**, 361–374 (2011).
[11]M. L. Da Silva, V. Guerra, and J. Loureiro, "State-resolved dissociation rates for extremely nonequilibrium atmospheric entries," J. Thermophys. Heat Transfer **21**, 40–49 (2007).
[12]M. Panesi and A. Lani, "Collisional radiative coarse-grain model for ionization in air," Phys. Fluids **25**, 057101 (2013).
[13]E. Josyula and W. F. Bailey, "Vibration-dissociation coupling using master equations in nonequilibrium hypersonic blunt-body flow," J. Thermophys. Heat Transfer **15**, 157–167 (2001).
[14]M. G. Kapper and J. Cambier, "Ionizing shocks in argon. Part II: Transient and multi-dimensional effects," J. Appl. Phys. **109**, 113309 (2011).
[15]A. Munafò, M. G. Kapper, J. L. Cambier, and T. E. Magin, "Investigation of nonequilibrium effects in axisymmetric nozzle and blunt body nitrogen

flows by means of a reduced rovibrational collisional model," AIAA paper 2012–647, 2012.
[16]M. Panesi, Y. Babou, and O. Chazot, "Predictions of non-equilibrium radiation: Analysis and comparison with EAST experiments," AIAA Paper 2008–3812, 2008.
[17]M. W. Huo, M. Panesi, and E. T. Magin, "Ionization phenomena behind shock waves," in *Physical Phenomena in Shock Waves* (Springer, 2011).
[18]A. Munafò, M. Panesi, R. L. Jaffe, G. Colonna, A. Bourdon, and T. E. Magin, "QCT-based vibrational collisional models applied to nonequilibrium nozzle flows," Eur. Phys. J. D **66**, 188–198 (2012).
[19]H. Drawin, "Atomic cross-sections for inelastic electronic collisions," Report No. EUR-CEA-FC 236, 1963.
[20]P. Teulet, J. Sarrette, and A. Gomes, "Calculation of electron impact inelastic cross sections and rate coefficients for diatomic molecules," J. Quant. Spectrosc. Radiat. Transf. **62**, 549–569 (1999).
[21]W. Lotz, "Electron-impact ionization cross-sections and ionization rate coefficients for atoms and ions from hydrogen to calcium," Z. Phys. **216**, 241–247 (1968).
[22]P. Teulet, J. Sarrette, and A. Gomes, "Collisional-radiative modelling of one- and two-temperature air and air-sodium plasmas at atmospheric pressure with temperatures of 2000-12000 K," J. Quant. Spectrosc. Radiat. Transf. **70**, 159–187 (2001).
[23]M. Capitelli, C. M. Ferreira, B. F. Gordiets, and A. I. Osipov, *Plasma Kinetics in Atmospheric Gases* (Springer, 2000).
[24]I. Kossyi, A. Y. Kostinsky, A. A. Matveyev, and V. P. Silakov, "Kinetic scheme of the non-equilibrium discharge in nitrogen-oxygen mixtures," Plasma Sources Sci. Technol. **1**, 207–220 (1992).
[25]C. Park, R. L. Jaffe, and H. Partridge, "Chemical-kinetic parameters of hyperbolic earth entry," J. Thermophys. Heat Transfer **15**, 76–90 (2001).
[26]D. Bose and G. V. Candler, "Thermal rate constants of the $N_2 + O \rightarrow NO + N$ reaction using ab initio $^3A''$ and $^3A'$ potential-energy surfaces," J. Chem. Phys. **104**, 2825–2833 (1996).
[27]D. Bose and G. V. Candler, "Thermal rate constants of the $O_2 + N \rightarrow NO + O$ reaction based on the $^2A'$ and $^4A''$ potential-energy surfaces," J. Chem. Phys. **107**, 6136–6145 (1997).
[28]C. O. Laux and C. H. Kruger, "Arrays of radiative transition probabilities for the N_2 first and second positive, NO beta and gamma, N_2 first negative and o_2 schumann-runge band systems," J. Quant. Spectrosc. Radiat. Transf. **48**, 9–24 (1992).
[29]L. V. Gurvich, *Thermodynamic Properties of Individual Substances* (CRC Press, 1994).
[30]V. Giovangigli, *Multicomponent Flow Modeling* (Birkhäuser, 1999).
[31]G. V. Candler and R. W. MacCormack, "Computation of weakly ionized hypersonic flows in thermochemical nonequilibrium," J. Thermophys. Heat Transfer **5**, 266–273 (1991).
[32]O. Knab, H.-H. Frhühauf, and E. Messerschmid, "Uranus/CVCV model validation by means of thermochemical nonequilibrium nozzle airflow calculations," in Proceedings of the 2nd European Symposium on Aerothermodynamics for Space Vehicles (ESA Publication Division, The Netherlands, 1992).
[33]A. Bourdon and P. Vervisch, "Electron-vibration energy exchange models in nitrogen plasma flows," Phys. Rev. E **55**, 4634–4641 (1997).
[34]S. O. Macheret, A. A. Fridman, I. V. Adamovich, J. W. Rich, and C. E. Treanor, "Mechanism on nonequilibrium dissociation of diatomic molecules," AIAA paper 1994–1984, 1994.
[35]M. L. Da Silva, V. Guerra, and J. Loureiro, "A review of non-equilibrium dissociation rates and models for atmospheric entry studies," Plasma Sources Sci. Technol. **18**, 034023 (2009).
[36]M. L. Da Silva, V. Guerra, and J. Loureiro, "Nonequilibrium dissociation processes in hyperbolic atmospheric entries," J. Thermophys. Heat Transfer **21**, 303–310 (2007).
[37]J. H. Ferziger and H. G. Kaper, *Mathematical Theory of Transport Processes in Gases* (North-Holland Publishing Company, 1972).
[38]B. Graille, T. E. Magin, and M. Massot, "Modeling of reactive plasmas for atmospheric entry flows based on kinetic theory," in Proceedings of the Summer Program, (Center for Turbulent Reasearch, Stanford, 2008).
[39]M. S. Liou, "A sequel to AUSM: $AUSM^+$," J. Comput. Phys. **129**, 364–382 (1996).
[40]A. Lani, "An object oriented and high-performance platform for areothermodynamics simulations," Ph.D. dissertation (Univesité Libre de Bruxelles, Bruxelles, Belgium, 2009).
[41]C. Hirsch, *Numerical Computation of Internal and External Flows* (Wiley, New York, 1990).
[42]Y. Saad, *Iterative Methods for Sparse Linear Systems* (SIAM, 2003).
[43]B. van Leer, "Towards the ultimate conservative difference scheme," J. Comput. Phys. **32**, 101–136 (1979).
[44]G. D. van Albada, B. van Leer, and W. W. Roberts, "A comparative study of computational methods in cosmic gas dynamics," Astron. Astrophys. **108**, 76–84 (1982).
[45]A. Lani, T. Quintino, D. Kimpe, H. Deconinck, S. Vandewalle, and S. Poedts, "The COOLFluiD framework: Design solutions for high-performance object oriented scientific computing software," in *Computational Science ICCS 2005*, LNCS 3514 Vol. 1, edited by P. M. A. S. V. S. Sunderan, G. D. van Albada, J. J. Dongarra, and Emory University (Springer, Atlanta, GA, USA, 2005), pp. 281–286.
[46]A. Lani, T. Quintino, D. Kimpe, H. Deconinck, S. Vandewalle, and S. Poedts, "Reusable object-oriented solutions for numerical simulation of PDEs in a high performance environment," Sci. Program. **14**, 111–139 (2006).
[47]M. Panesi, "Modeling of nonequilibrium plasma flows for re-entry applications," Ph.D. dissertation (Università degli Studi di Pisa, Pisa, Italy, 2009).
[48]T. G. Owano, M. H. Gordon, and C. H. Kruger, "Measurements of the radiation source strength in argon at temperatures between 5000 and 10000 K," Phys. Plasmas **2**, 3184 (1990).
[49]M. G. Gordon, "Nonequilibrium effects in a thermal plasma," Ph.D. dissertation (Stanford University, San Francisco, CA, 1992).
[50]D. A. Benoy, J. A. M. van der Mullen, and D. C. Schram, "Radiative energy loss in a non-equilibrium argon plasma," J. Phys. D **26**, 1408–1413 (1993).
[51]R. J. Gessman, C. O. Laux, and C. Kruger, "Experimental study of kinetic mechanisms of recombining atmospheric pressure air plasmas," AIAA paper 1997–2364, 1997.
[52]C. O. Laux, "Optical diagnostics and radiative emission of air plasmas," Ph.D. dissertation (Stanford University, San Francisco, CA, 1993).
[53]L. Pierrot, L. Yu, R. J. Gessman, C. O. Laux, and C. Kruger, "Collisional-radiative modeling of nonequilibrium effects in nitrogen plasmas," AIAA paper 1999–3478, 1999.
[54]C. O. Laux, "Radiation and nonequilibrium collisional radiative models," in *Physico-chemical Models for High Enthalpy and Plasma Flows*, Lecture Series (von Karman Institute for Fluid Dynamics, 2006).
[55]D. G. Fletcher, "Nonintrusive diagnostic strategies for arcjet stream characterization," in *Measurement Techniques for High Enthalpy Plasma Flows*, Lecture Series (von Karman Institute for Fluid Dynamics, 1999).
[56]V. A. Gorelov, M. K. Gladyshev, A. Y. Kireev, I. V. Yegorov, Y. A. Plastinin, and G. F. Karabadzhak, "Experimental and numerical study of nonequilibrium ultraviolet NO and N_2^+ emission in shock layer," J. Thermophys. Heat Transfer **12**, 172–179 (1998).